ADVANCED FUNCTIONAL MATERIALS
www.afm-journal.de

Dual-Modal Sensing Platform Based on Flexible GaN Microdisk Lasers on PDMS Substrate

Hongkun Zhong, Lilong Ma, Tao Yang, Quan Peng, Leiying Ying, Yang Mei, and Baoping Zhang**

Whispering gallery mode (WGM) micro-nano resonant cavities have demonstrated significant potential in high-sensitive sensing applications due to their compact footprint, rapid response, and high Q factor etc. Nevertheless, fabrication of high-performance WGM devices suitable for multifunctional sensing remains challenging due to complicated fabrication process and material limitations. Furthermore, most existing devices are constrained to a single modal sensing capability and rigid substrate, limiting their multifunctionality and flexibility. This study presents an innovative approach to fabricating GaN-based microdisks on flexible PDMS substrate via a secondary substrate transfer technique, overcoming critical fabrication challenges. The active microcavity achieves a Q factor up to 10 923. The lasing spectrum in green spectral region can be precisely tuned not only by modulating the strain in the PDMS substrate, but also by altering the refractive index of the surrounding material, showing dual-modal sensing capability. Experimental results demonstrate that the sensitivity of sensing about the strain and the refractive index are 0.08 nm/mm^{-1} and 666.9 nm/RIU, respectively. The detection limit of the refractive index sensor is as low as 5.4×10^{-6} RIU. This study provides a novel dual-modal flexible sensing platform which is promising in strain sensing, water quality monitoring, laser dynamic modulation, and tactile sensing.

1. Introduction

Micro-nano cavity based optical sensors have attracted much attention in sensing research in recent years, attributing to their superior detection capability. Among different type of microcavities, whispering gallery mode (WGM) cavities are especially suitable for sensing applications. WGMs are usually distributed at peripheral area of the microcavity, and the evanescent field of the cavity modes can be sensitively influenced by the change of their surrounding environments, boosting the sensing capability. WGM microcavities are also featured with high sensitivity,[1] high Q-factor,[2,3] easy integrability,[4] rapid response,[5] and compact device size.[6] And they have been extensive used in intracellular exploration,[7] label-free single-molecule detection,[8] molecular electrostatic surface analysis,[9] Tau protein detection,[10] glucose monitoring,[11] urine pH test,[12] sucrose concentration analysis,[13] and cardiac tissue contractility measurement.[14] At present, most WGM microcavities for sensing application are based on Silicon nitride (SiN) material because of the chemical stability, low optical loss, and excellent mechanical properties.[15,16] However, SiN based microcavities are passive and cannot generate light directly. They usually need to be integrated with an external laser source through complicated coupling system. In addition, SiN based microcavities are typically operating in the near-infrared spectral region, limiting their application in water environment sensing. It is well established that there exists low loss windows in water at blue and green spectral band.[17] Moreover, many microscopic biological markers like nerve cells and hemoglobin in water environments exhibit higher responsiveness to visible light.[18,19] Therefore, it is essential to develop high performance sensing platform based on WGM microcavities operating in visible spectral band.

Microcavities fabricated by GaN-based semiconductors with wide and tunable bandgap are ideal choices to address the above problems. The emission wavelength of GaN based materials can cover the whole visible region,[20–23] and they are also excellent gain medium for visible microcavity lasers.[24–26] Therefore, high performance GaN based microcavity lasers can be directly used for sensing applications in visible light region. To date, reports on GaN-based WGM micro laser sensors are still rare. Pan et al. fabricated GaN-based microwire lasers on flexible PET substrates, and lasing peak at ultraviolet band can be modulated through substrate mechanical modifications, realizing the function of strain sensing.[27] Hu et al. fabricated a tubular WGM laser based on InGaN/GaN quantum wells on a flexible PDMS substrate. By

H. Zhong, L. Ma, T. Yang, Q. Peng, L. Ying, Y. Mei, B. Zhang
Laboratory of Micro/Nano-Optoelectronics
Department of Micro Electronic and Integrated Circuits
Xiamen University
Xiamen 361005, China
E-mail: meiyang@xmu.edu.cn; bzhang@xmu.edu.cn
B. Zhang
Institute of Nanoscience & Applications
Southern University of Science and Technology
Shenzhen 518055, China

The ORCID identification number(s) for the author(s) of this article can be found under https://doi.org/10.1002/adfm.202501566

DOI: 10.1002/adfm.202501566

bending the PDMS substrate, the shape of the microtubular was changed, inducing the shift of the lasing peak and the function of strain sensing.[28] Choi et al. developed GaN-based microdisk lasers on PDMS substrates using laser lift-off (LLO) and microsphere lithography (MSL), achieving controlled shift of the blue lasing peak via substrate deformation.[29] Furthermore, Gu et al. fabricated GaN-based ultraviolet microdisk lasers on PET flexible substrate with wavelength tunable characteristics.[30] The tunable lasing wavelength governed by the deformation of flexible substrates underscores the exceptional micro strain optical sensing capabilities of GaN-based WGM microcavity lasers. The integration of WGM microcavity devices with flexible films offers not only substantial potential in strain optical sensing, but also promising for evanescent field related environmental refractive index optical sensing. However, fabricating high-quality flexible devices is still difficult because of the uneven stress distribution between the epitaxial materials and the flexible films. Moreover, existing studies about flexible GaN based WGM lasers are limited to a single modal strain optical sensing, and there is no report about refractive index optical sensing, especially for water environment monitoring.

In this study, we present a new method to fabricate high-performance flexible GaN-based microdisk lasers on PDMS substrate, and verified the capability of dual-modal sensing of both strain and environmental refractive index. The flexible microdisk laser shows a low threshold energy density of 312.31 μJ cm^{-2} and high Q factor of 10 923 in blue-green spectral band. While tensile stress was applied to the PDMS substrate to modulate the strain state of the microdisk, the lasing wavelength of the microdisk can be linearly tuned. The stress state inside the microdisk lasers was systematically studied through Raman characterization. These unique features enable the flexible GaN-based microdisk laser to function not only as a conventional laser light source but also as a high-performance micro strain optical sensor. Furthermore, by modulating the refractive index of the surrounding environment, the lasing spectrum of the microdisk laser exhibited distinct tunability, making it suitable for monitoring environmental changes and operating as a micro refractive index optical sensor. The sensing capability of the device was verified in NaCl solution, and mass concentrations as low as 0.01% can be detected, achieving a detection limit in the low concentration range (0%–0.1%) down to 5.4×10^{-6} RIU and sensitivity up to 666.9 nm/RIU, which are among the best values of the previously reported devices.[31,32] The flexible GaN-based microdisk lasers in this study can independently achieve high-performance dual-modal sensing without integration of multiple single-function sensors, which greatly simplified the sensing system.[33–35] Our study provides effective support for solving multifunctional optical sensing applications.

2. Results and Discussion

2.1. Device Fabrication

The epitaxial wafer used to fabricate the microdisk lasers was grown on a (0001) crystal-oriented sapphire substrate via a metal-organic chemical vapor deposition (MOCVD) system. The active region contains eight pairs of $In_{0.28}GaN$/GaN (3 nm/15 nm) multi-quantum wells (MQWs) emitting in green spectra region. The MQW structure is commonly used as the active region of GaN-based lasers for high-performance lasing.[24–26] The detailed structure of the epi-wafer was given in the Figure S1 (Supporting Information). **Figure 1a** illustrates the fabrication process of the flexible GaN-based microdisk lasers. Initially, a SiO_2 sacrificing layer was deposited on the GaN epitaxial wafer and small holes were opened (Step 1). The sample was then flip-chip bonded on a temporary Si substrate through adhesive bonding, and the holes in the SiO_2 sacrificing layer were filled by the bonding material (Step 2). Subsequently, the sapphire substrate was removed via an excimer LLO technique, and the cavity was thinned to 680 nm through chemical mechanical polishing (CMP) (Step 3). The surface of the polished GaN epitaxial layer exhibits atomic level flatness with a root mean square (RMS) roughness of 0.36 nm in a 10×10 μm^2 area, as shown in Figure 1b. The flat surface and sidewall of the microdisk are essential to realize low threshold lasing, narrow linewidth and high Q factor. The mesa of the microdisk was then generated by inductively coupled plasma (ICP) etching, and the etching process was stopped after the expose of the SiO_2 sacrificing layer (Step 4). The SiO_2 sacrificing layer was removed by a buffered oxide etch (BOE) solution containing 49% hydrofluoric acid (HF) at a constant temperature of 40 °C. The etching time is 8 minutes, yielding the semi-suspended "mushroom type" GaN-based microdisk lasers (Step 5). The microdisks were supported by the pillars generated from the bonding material in Step 2. Finally, the microdisks were attached to a PDMS substrate, and can be easily peeled off from the Si substrate and supporting pillars (Step 6). The scanning electron microscopy (SEM) images and the overall bending image of the flexible microdisk lasers are provided in Figure 1c,d. The microdisks are tightly attached to the surface of the PDMS substrate.

2.2. Optical Properties of Microdisk Lasers

A micro-photoluminescence (μ-PL) measurement system was employed to investigate the optical and sensing properties of the flexible GaN microdisk lasers, and the schematic diagram of the system is presented in **Figure 2a**. A CryLas FTSS-355 Q1 pulsed laser (wavelength: 355 nm, pulse width: 1 ns, repetition frequency: 15 kHz) was utilized as the pump light source. The laser beam was focused onto the sample surface using a microscope objective (NA0.35, 50X). Stimulated emission from the microdisk was collected by the same objective and directed into a spectrometer equipped with an electrically cooled charge-coupled device (CCD) as the detector. Figure 2b shows the images of a flexible GaN microdisk laser on PDMS substrate before and after lasing, with the device's emission intensity increasing rapidly, and emission color changing from green to cyan. Figure 2c presents the typical output spectrum of a GaN microdisk laser with diameter of 18 μm, where the insets illustrate the corresponding luminescence picture. Under pump energy density of 252.97 μJ cm^{-2}, the microdisk exhibits spontaneous emission in green without lasing modes. When the energy density increases to 324.40 μJ cm^{-2}. stimulated emission takes place, producing a sharp lasing peak at 491.53 nm. The optical field is well confined in the peripheral region of the microdisk and gets much stronger beyond the threshold, demonstrating the oscillation of WGM modes. The linewidth of the WGM mode is as narrow as 0.045 nm, corresponding to a

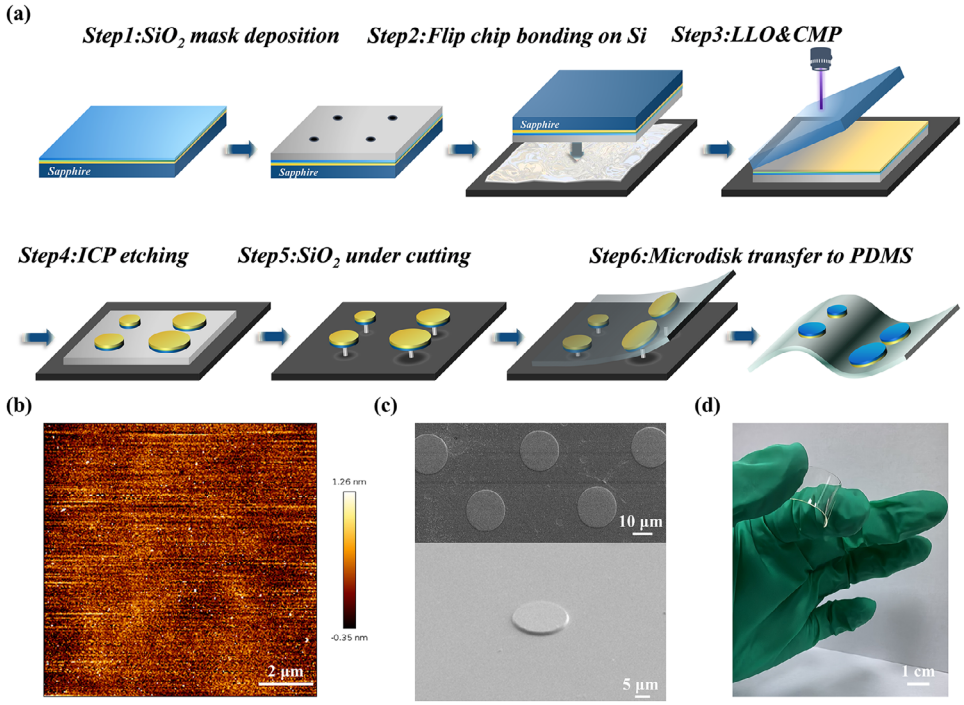

Figure 1. a) Fabrication processes of GaN microdisk lasers on PDMS substrate. b) Atomic force microscope (AFM) image of the GaN-based microdisk surface. c) Top-view and side-view SEM images of microdisk lasers. d) Image of the flexible microdisk lasers under bending.

high Q factor of 10 923, as shown in Figure 2d. Figure 2e illustrates the PL intensity and linewidth of the microdisk as a function of pump energy density. The typical "S" shape of the output behavior and the abrupt reduction of the linewidth demonstrate the lasing action. The threshold excitation energy is estimated to be 312.31 μJ cm^{-2}, and the spontaneous coupling factor β was fitted to be 0.016. The above features of flexible GaN-based microdisk lasers in green spectral region including high Q factor and low threshold are well suited for optical sensing applications.

2.3. Strain Optical Sensing of the Flexible Microdisk Lasers

To investigate the strain-dependent optical properties of GaN-based microdisk lasers, a displacement testing platform was designed, as illustrated in **Figure 3**a. The detailed measurement system is given in Figure S2 in the Supporting Information. Optical properties of the GaN microdisk laser under different strains were measured by adjusting the stress applied to the flexible PDMS substrate. Figure 3b shows the emission of the microdisk lasers beyond lasing threshold under different substrate curvature, lasing characteristics can be well maintained under different strain states. Figure 3c,d depict the lasing spectra of the flexible microdisk laser under varying substrate curvature. It is evident that as the substrate curvature increases (corresponding to a decrease in the radius of curvature R), the wavelength of the microdisk laser exhibits a blueshift. Figure 3e illustrates the relationship between the lasing wavelength and substrate bending curvature (1/R), revealing a linear modulation of the lasing wavelength from 493.37 nm to 493.28 nm. The lasing thresholds and linewidths of the microdisk laser at different curvature radii are similar, which are given in Table S1 of the Supporting Information. The model to calculate the curvature radius and tensile stress are provided by Figure S3 (Supporting Information).

With increasing substrate bending, the radius of curvature decreases, causing slight deformation of the microdisk. The microdisk and PDMS substrate are tightly adhered to each other during the deformation process. The deformation of the microdisk results in a reduced effective optical path length of the WGMs inside the microdisk, making the resonate wavelength of the WGMs shift to a shorter wavelength. Similar phenomenon have also been reported in other GaN based flexible lasers.[28,29] The sensitivity of the emission peak position to substrate deformation highlights the remarkable strain-optical sensing capabilities of flexible GaN-based microdisk lasers. The sensitivity (S) here is defined as the ratio of the luminescence wavelength shift to the bending curvature.[29] The dashed line in Figure 3e represents the linear fitting result, yielding a sensitivity value of $S = 0.08$ nm/mm^{-1}. The sensitivity here can be further improved by reducing the cavity size of the microdisk laser. It is well established that shorter cavities exhibit more pronounced mode shifts for the same change in cavity length.[36] However, smaller microdisk lasers suffer from significant optical losses, which increase the lasing threshold. Smaller cavities also exhibit broader linewidth or a reduced Q-factor, diminishing the actual detection resolution. Therefore, there is a tradeoff between the sensitivity and detection resolution for microdisk laser based optical sensors. The linewidth of the flexible lasers in this study are featured with impressively narrow linewidth of 0.045 nm, and a high Q-factor of 10 923. The combination of a high Q-factor and a narrow linewidth markedly enhances the detection accuracy of lasing peak shifts in microdisk lasers, even under minute

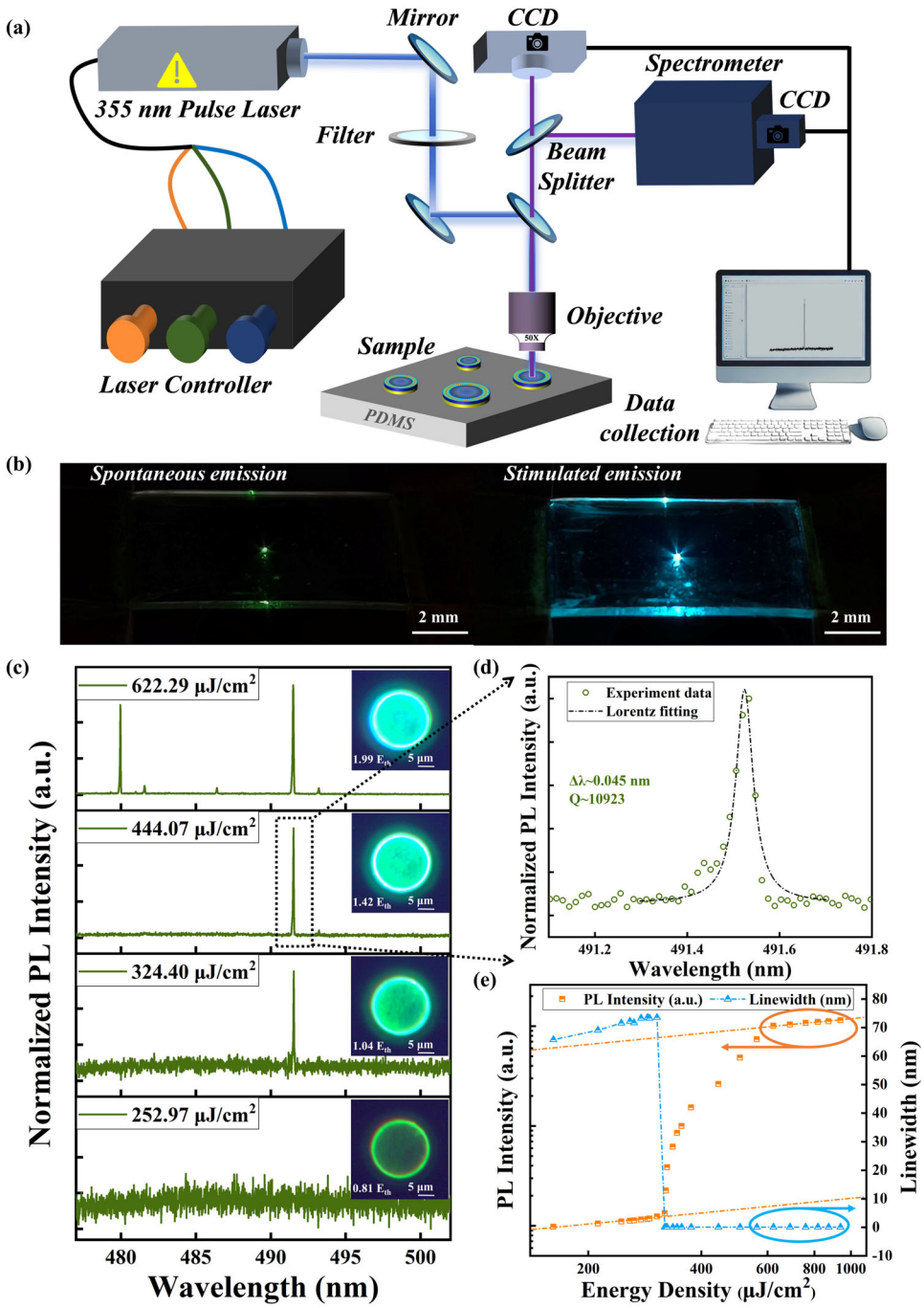

Figure 2. a) Schematic of the μ-PL measurement system. b) Images before and after lasing of a microdisk laser. c) Normalized PL spectra recorded under varying pump energy levels at room temperature. The inset depicts luminescence images of the microdisk below and above the lasing threshold. d) Q-factor versus linewidth profiles derived from Lorentz curve fitting. e) PL intensity and linewidth as a function of pump energy density.

substrate strain variation. The flexible GaN-based microdisk lasers also have excellent bending recovery properties when we continuously and dynamically bend and recover the substrate, and the lasing wavelength of the microdisk can respond instantaneously to the bending of PDMS, which can be demonstrated by Figure 3f. Due to the limitation of the manually adjusted measurement system, we can only qualitatively conclude that the microdisk responds well to the dynamic strain, and it is still difficult at present to analyze the response time and potential hysteresis very accurately. This can be solved in the future work by upgrade the measurement system and introduce an automatic strain regulation system.

Raman characterization was used to investigate the strain inside the microdisk due to substrate deformation. When tensile stress is applied to the material, the distance between atoms increases, resulting in the frequency of lattice vibrations

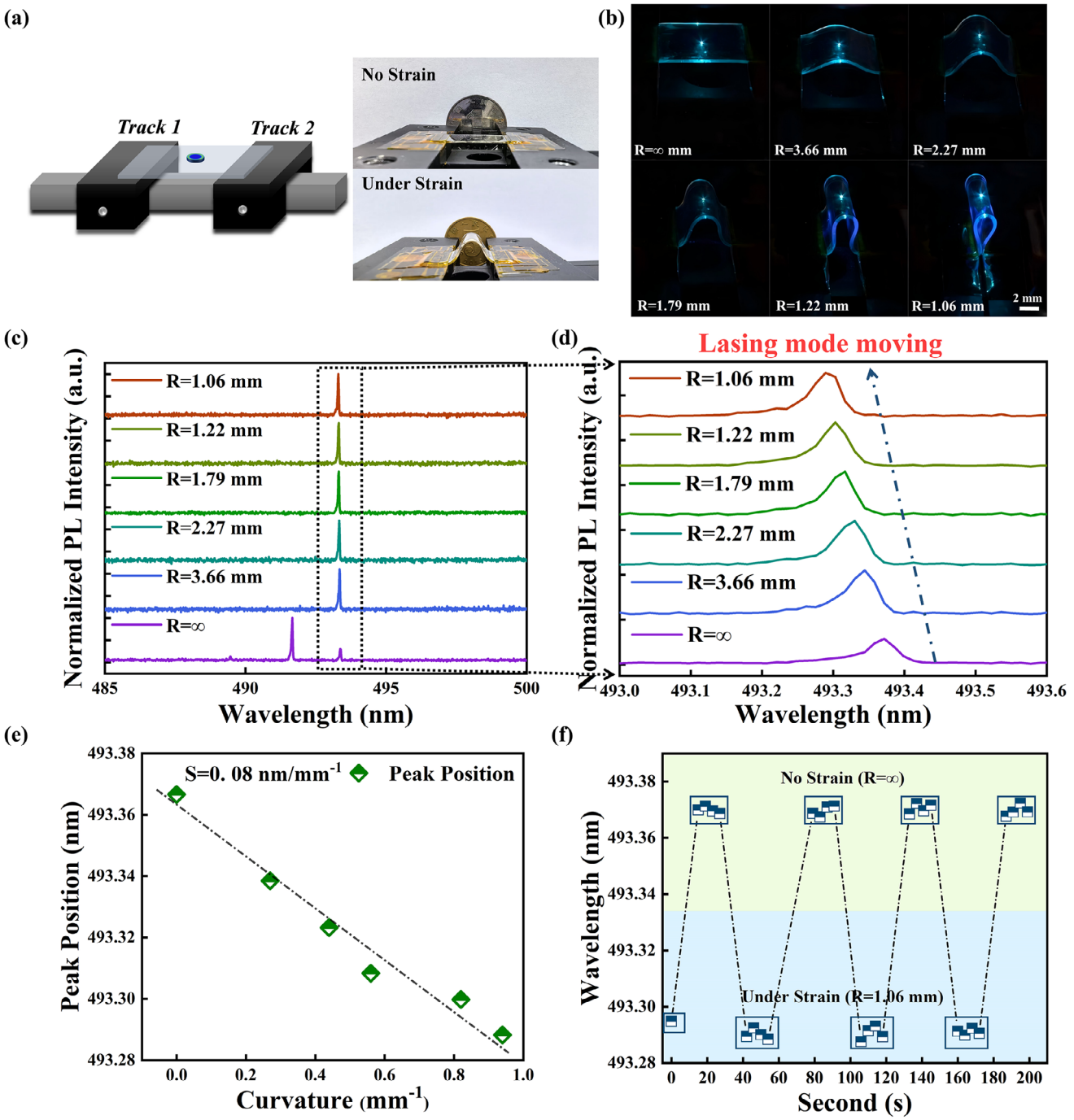

Figure 3. a) Movable test displacement stage. b) Macroscopic excitation phenomena of microdisk laser under varying bending curvature of the substrate. c) Normalized PL spectra of the substrate recorded at room temperature under different bending curvature. d) Magnified view of the normalized PL spectra within the dashed box in (c). e) The relationship between microdisk's excitation peaks and the bending curvature (1/R). (f) Variation of lasing wavelength of the flexible GaN microdisk laser before and after bending for several times (From $R = \infty$ to $R = 1.06$ mm).

decreases, and the phonon mode characteristic peaks shift to the low-frequency region.[27] By evaluating the high phonon mode peak (E_{2h}) shift of GaN, we can obtain the information of the strain inside the film.[37] We employed a 633 nm laser as the excitation source during Raman measurement, and recored the Raman spectra at five points along the diameter of the microdisk, as shown in **Figure** 4a. Figure 4b shows the normalized Gaussian-fitted Raman spectra of each point when the PDMS substrate was under the unstrained flat state. It can be observed that the E_{2h} peak of GaN shows no obvious shift among different positions. The Raman shift is around 563.8 cm^{-1}, smaller than the ω_0 = 567.5 cm^{-1} of freestanding bulk GaN material. This indicates

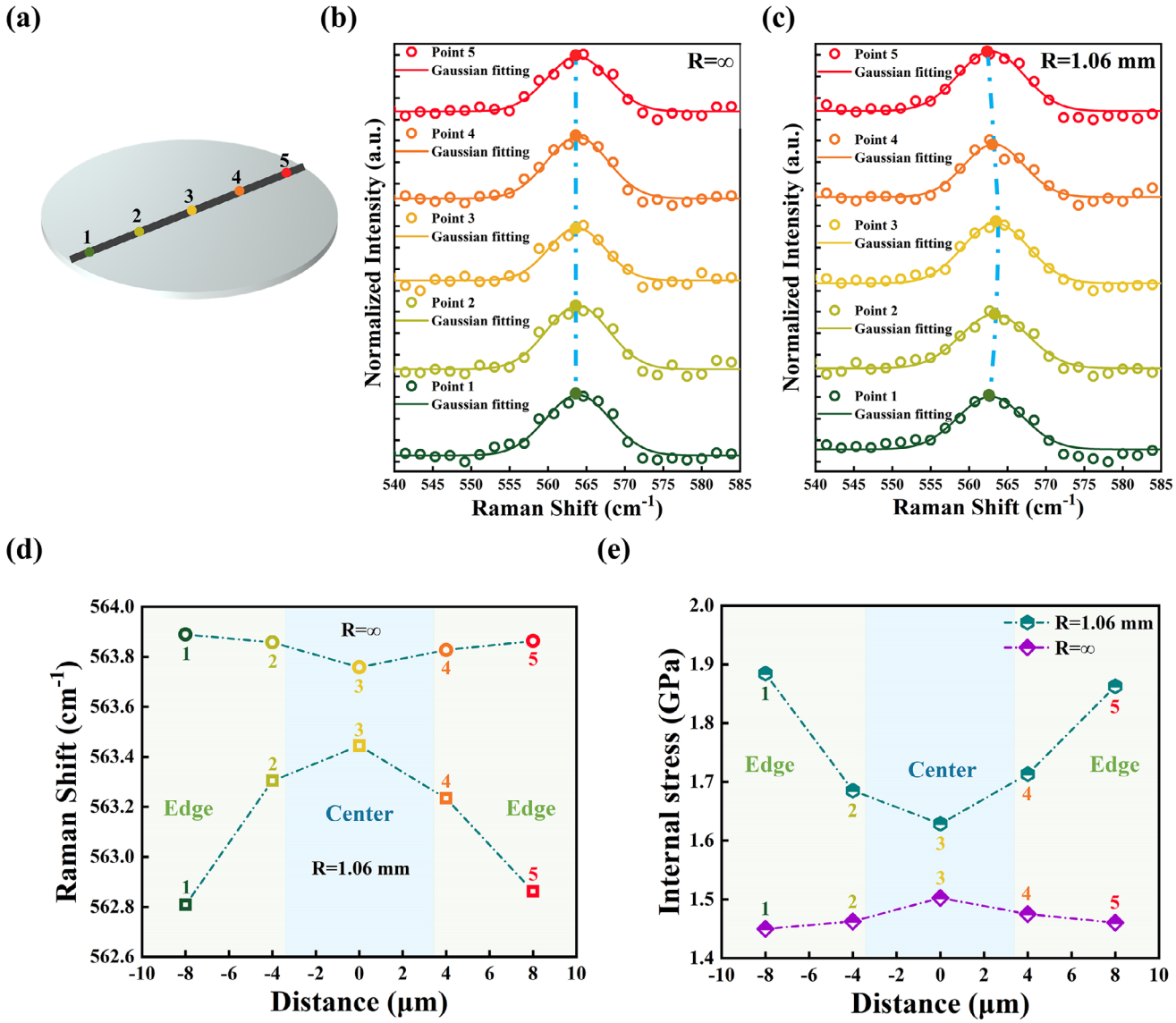

Figure 4. a) Distribution of test points along the diameter of the microdisk surface (Point1-poin5). b) Curvature radius $R = \infty$, normalized Gaussian-fitted Raman spectra of the PDMS substrate from point 1 to point 5. c) Curvature radius $R = 1.06$ mm, normalized Gaussian-fitted Raman spectra of the PDMS substrate from point 1 to point 5. d) E_{2h} Phonon frequency distribution from point 1 to point 5 under different stress states of the PDMS substrate. e) Internal stress from point 1 to point 5 under different stress states of the PDMS substrate.

that due to the lattice mismatch between InGaN and GaN films, there exists in-plane tensile stress within the GaN of the fabricated microdisk.[37] Figure 4c presents the normalized Gaussian-fitted Raman spectra of the GaN microdisk with external tensile stress when the PDMS substrate was deformed under curvature radius of $R = 1.06$ mm. The Raman peaks of E_{2h} from the edge of the microdisk shift towards a lower wavenumber when compared with the central region. Figure 4d shows the comparation of the Raman shift of the 5 points on GaN microdisk when the PDMS substrate was under flat and bending condition, respectively. When the substrate is in a strained state with a curvature radius $R = 1.06$ mm, the E_{2h} peak values at the test points are symmetrically distributed around the center point. From point 3 to point 1, the E_{2h} phonon frequency decreases from 563.4 cm^{-1} to 562.8 cm^{-1}, and the E_{2h} phonon frequencies at all points are lower than flat state of 563.8 cm^{-1}. This means that the tensile stress in GaN microdisk under bending condition is larger than that of flate state, and the stress distribution is different along the diameter of the microdisk. The stress inside the microdisk can be calculated by the equation:

$$\Delta\omega = a_{GaN}\sigma_{xx} \tag{1}$$

where $\Delta\omega$ is the shift of the phonon frequency with respect to that of stress-free GaN (567.5 cm^{-1}), a_{GaN} is the Raman stress coefficient of GaN (2.49 cm^{-1} GPa^{-1}), and σ_{XX} is the in-plane stress.[37] Figure 4e shows the tensile stress distribution inside GaN microdisk under flat and bending condition, respectively. The

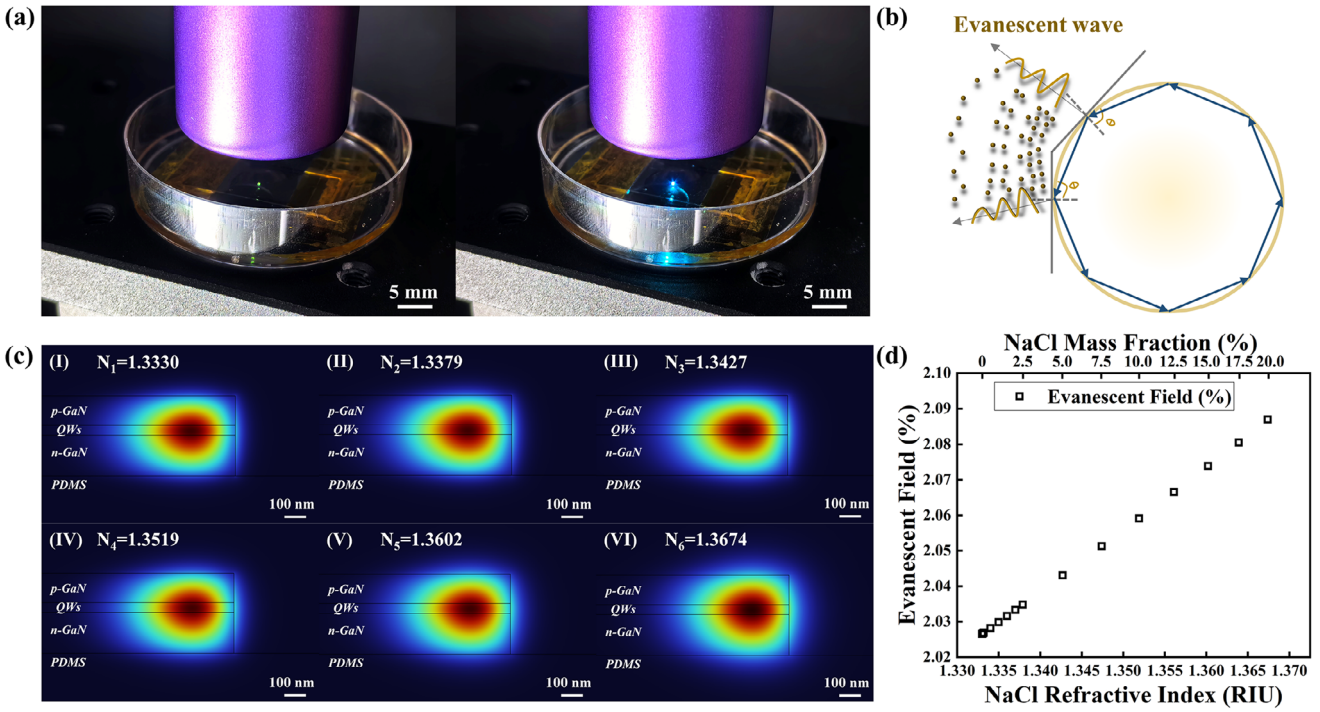

Figure 5. a) Macroscopic luminescence phenomena observed in a microdisk laser before and after lasing within NaCl solution. b) The mechanism underlying the internal resonant mode operation of the microdisk laser. c) FEM simulation of the optical field distribution in a flexible GaN-based microdisk laser immersed in NaCl solutions with increasing refractive index ($N_1 < N_2 < N_3 < N_4 < N_5 < N_6$). d) The functional relationship between the evanescent field proportion of the microdisk laser and the solution's refractive index under varying NaCl concentrations.

tensile stress in GaN microdisk at each point is higher under bending condition than that of flate state, duing to the external tensile stress caused by the deformation of the substrate. In addition, the stress distribution along the diameter of the microdisk is a little diffferent from center to edge under bending condition. The tensile stress increased from 1.63 GPa at point 3 to 1.88 GPa at point 1. This can be caused by the adhesion forces between PDMS substrate and GaN microdisk, as well as the local deformation of the PDMS substrate. The full Raman spectrum of GaN microdisk on PDMS substrate and the measurement system are provided in Figure S4 (Supporting Information).

2.4. Refractive Index Optical Sensing of the Flexible Microdisk Lasers

To investigate the optical properties of GaN-based microdisk lasers under varying environmental conditions with different refractive index, the PDMS substrate was fixed within a plastic petri dish and immersed in NaCl solutions with different concentration. The experiment was conducted in clean room and the container of the NaCl solution was placed on a copper heatsink. The room temperature and humidity were controlled to be 25 °C and 40% by air conditioner system. Because the microdisk is attached on PDMS substrate and immersed in NaCl solution, the periphery sidewall and top surface of the microdisk are contact directly with the NaCl solution except for the bottom surface. The detailed measurement system is given in Figure S5 in the Supporting Information. **Figure** 5a illustrates the macroscopic images of a microdisk laser immersed in NaCl solution before and after lasing, where a transition from weak green light to intense cyan occurs as the pumping energy increases. Lasing characteristics can be well maintained for the flexible microdisk lasers within the solution. Figure 5b presents a schematic representation of the internal resonance mode mechanism within the microdisk laser. The WGMs inside a microdisk laser are generated by the total internal reflection at sidewall and surface, and are distributed at peripheral region of the microdisk. A fraction of the resonate mode will penetrate into the surrounding medium, allowing the electromagnetic field to extend a short distance and propagate along the interface, forming the evanescent wave. The exceptional locality and sensitivity to refractive index change of evanescent wave make it a valuable tool for detecting subtle surrounding environmental changes. The environmental changes alter the evanescent field distribution, consequently affecting the WGMs of the microdisk laser. The finite element method (FEM) was employed to simulate the mode distribution of the microdisk lasers when immersed in NaCl solutions with varying concentrations, as shown in Figure 5c. Specific information of the model used for simulation is given in Figure S6 in the Supporting Information. The refractive index of NaCl solutions increases with increasing concentration, reducing the refractive index difference between the GaN based microdisk and the surrounding environment. Consequently, an increasing proportion of optical field are distributed outside the microdisk. The proportion of the evanescent field increases progressively with the rising refractive index of the NaCl solution, as illustrated in Figure 5d. This means increased leakage of optical wave energy from the extended

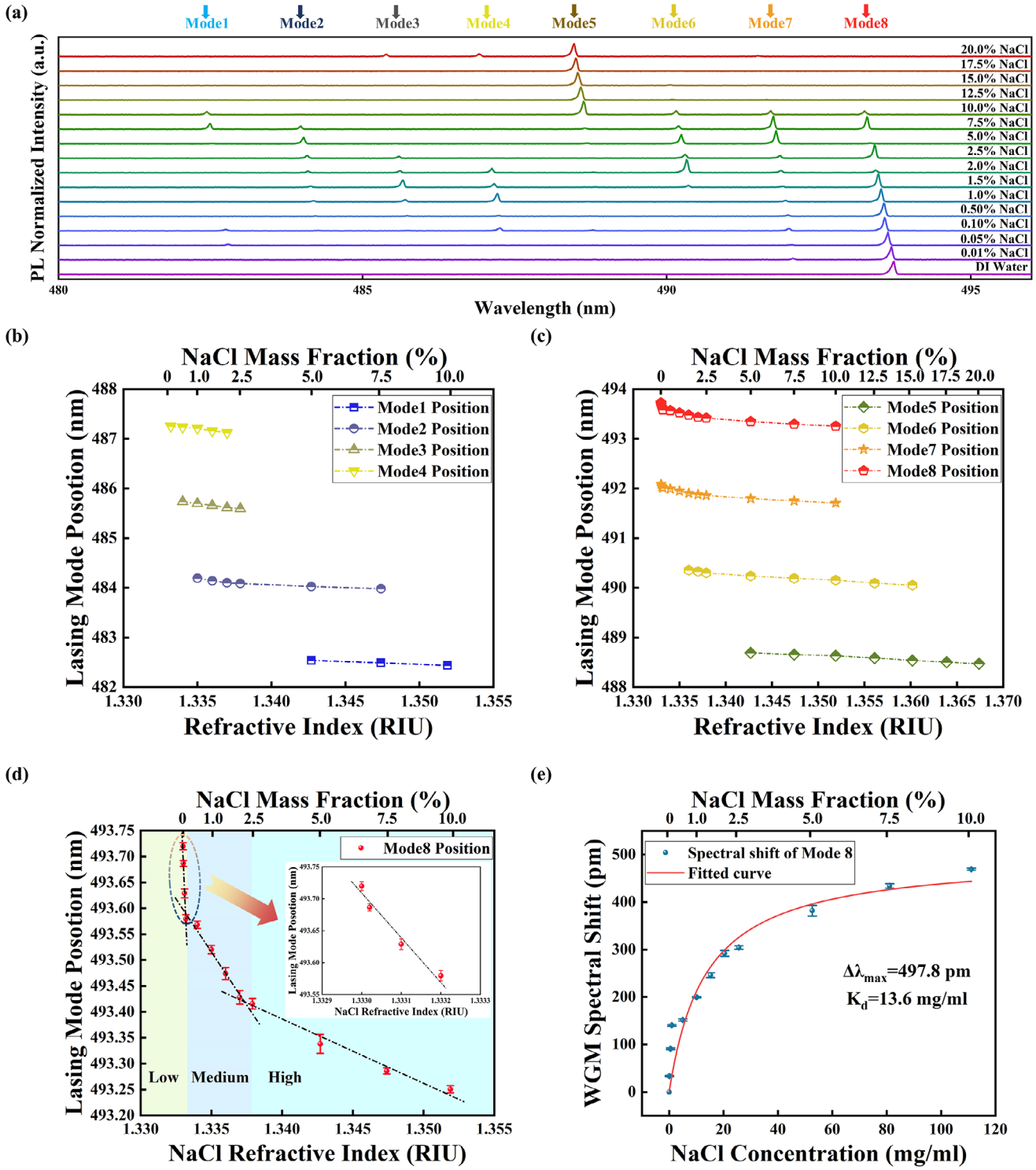

Figure 6. a) Normalized PL spectra of a microdisk laser at varying NaCl solution concentrations. The wavelength of the lasing modes b) Mode 1–Mode 4, and c) Mode 5–Mode 8 as a function of the refractive index of the solution. d) The wavelength of Mode 8 as a function of the refractive index of the solution. e) Dependence of the spectral shift of Mode 8 on the concentration of NaCl solution.

Table 1. Sensitivity of Modes 1 to Mode 8 at their respective concentration ranges.

	Low [0%–0.1%] S [nm/RIU]	Medium [0.1%–2.5%] S [nm/RIU]	High [2.5%–20.0%] S [nm/RIU]
Mode1	/	/	10.9
Mode2	/	36.9	11.3
Mode3	/	37.3	/
Mode4	/	35.0	/
Mode5	/	/	9.1
Mode6	/	28.0	10.9
Mode7	427.9	34.1	10.8
Mode8	666.9	38.2	11.7

portion of the optical mode in the microdisk resonator into the external medium, the effective refractive index experienced by the optical mode decreases. Based on the resonate condition $m\lambda = 2\pi r n_{eff}$, the excitation wavelength of the microdisk laser decreases correspondingly.[38]

The optical properties of GaN microdisk lasers in varied environments including deionized water and NaCl solutions with mass fractions ranging from 0.01% (100 µg ml^{-1}) to 20% (250 mg ml^{-1}) were experimentally measured. We repeated the solution concentration dependent PL measurement for 4 times to guarantee the reliability and stability of the experimental data. Spectral and data error analysis of the repeatability experiments are provided by Figure S7, Tables S3,S4 in the Supporting Information. **Figure 6**a presents the normalized PL spectrum of a microdisk laser under varying NaCl solution concentrations. Evidently, as the concentration increases, the lasing mode exhibits a gradual blue shift. To investigate the evolution of the lasing peaks in greater detail, the eight lasing peaks in the spectrum shown in Figure 6a were labeled sequentially from left to right as Mode 1 to Mode 8. All peaks show a noticeable blue shift with increasing concentration of the NaCl solution and few peaks disappeared and reappeared. The missing peaks in the normalized spectra are caused by mode competition, which is common in GaN based microdisk lasers with large diameter. After lasing, the multi-modes will compete to each other, and the slight fluctuation of carrier concentration in MQWs or the surrounding environment can cause the mode hopping.[39,40] Figure 6b,c illustrate the relationship between the wavelength of the lasing modes and the refractive index of the solution. Within distinct concentration ranges of the test solution, the blue shift of the lasing modes exhibits a consistent and predictable trend. Figure 6d shows the magnified data for Mode 8, and the response of the lasing peak can be clearly divided into three different region according to the mass concentration, which can be defined as low (0%–0.1%), medium (0.1%–2.5%), and high (2.5%–20%) mass concentration, respectively. The sensitivity "S" is defined as the ratio of the shift in lasing peak position "$\Delta\lambda$" to the change in the refractive index of the solution "Δn", expressed as $S = \Delta\lambda/\Delta n$.[41] By fitting the regional drift curves of each lasing mode in Figure 6b,c, the sensitivities of Modes 1 through 8 for the respective concentration ranges were determined and are presented in **Table 1**.

As demonstrated in Table 1, the detection sensitivity of the microdisk laser is notably higher in the low concentration region compared to the medium and high concentration region. And the sensitivity of mode 7 is slightly lower than that of mode 8 in the low concentration range. It is known that the first order WGMs obey the resonance condition $m\lambda = 2\pi r n_{eff}$, where λ is the resonate wavelength, m is the number of azimuthal modes, representing the number of standing wave periods formed in the circumferential direction of the microdisk, and n_{eff} is the effective refractive index of the optical modes. Mode 7 has a smaller resonate wavelength, therefore the mode order is larger than that of Mode 8 ($m_8 < m_7$). The intrinsic cause of the shift of the lasing modes with different NaCl concentration is the change of effective refractive index n_{eff} of the cavity modes, which changed the resonance condition. For a cavity mode with resonate wavelength of λ and a change of refractive index Δn, it will show a corresponding mode shift $\Delta\lambda$, where

$$m(\lambda + \Delta\lambda) = 2\pi r(n_{eff} + \Delta n) \tag{2}$$

and

$$m\Delta\lambda = 2\pi r\Delta n \tag{3}$$

Therefore, for a fixed refractive index variable Δn, WGMs with smaller azimuthal mode number will show a larger $\Delta\lambda$, then a larger sensitivity.

From Figure 6d, it can be seen that as the solution concentration increases, the blue shift of the lasing peak tends to saturate. In WGM-based biosensors, the adsorption and desorption processes of biomolecules on the sensor surface may induce alterations in the local refractive index, consequently influencing the resonance modes of light. The Langmuir isotherm model can be employed to characterize this process:

$$\Delta\lambda = \Delta\lambda_{max}\left(\frac{M}{K_d + M}\right) \tag{4}$$

where $\Delta\lambda$ is the spectral shift, $\Delta\lambda_{max}$ is the maximum spectral shift, K_d is the dissociation constant, and M is the analyte concentration.[42,43] When the target molecule interacts with the sensor surface, K_d governs the equilibrium state of the binding reaction.[44] When the concentration of the target molecule is below K_d, the binding reaction has not yet reached equilibrium; in this regime, even small fluctuations in concentration can significantly drive the reaction forward, resulting in more pronounced signal changes. The response of the microsensor to the concentration of NaCl solution in this study can also be very well fitted by the model in equation 4, as illustrated by the red solid line in Figure 6e. The increase in NaCl concentration results in a pronounced saturation effect. $\Delta\lambda_{max}$ and K_d can be fitted to be 497.8 pm and13.6 mg ml^{-1}, respectively. This study revealed that Mode 8 exhibits a sensitivity of up to 666.9 nm/RIU in the low concentration range, and the device demonstrates the capability to detect NaCl solution concentrations as low as 0.01%. Since GaN-based material is a kind of polar material, there exists negative charges on the surface of GaN grown along [0001] direction due to the spontaneous polarization.[45,46] The surface of the microsensor can attract Na^+ ion due to the coulomb attraction. Such mechanism of ionic adsorption on GaN surface has been widely used in GaN wet etching technology.[47,48] Therefore, there exists

Table 2. Comparison of DL value, sensitivity, linewidth, Q factor and analyte.

Device configurations	DL (RIU)	Sensitivity (nm/RIU)	Linewidth (nm)	Q factor	Analyte	Refs.
SiN Microring	$\sim 4.7 \times 10^{-4}$	384.6	~2.7	8610	NaCl	[31]
SiN Microring	$\sim 3.7 \times 10^{-5}$	91.0	~0.05	~75000	NaCl	[41]
Si_3N_4 Microring	$\sim 1.4 \times 10^{-5}$	64.2	/	~190000	NaCl	[50]
Si Microdisk	$\sim 8.0 \times 10^{-4}$	130.0	1.5	~12000	NaCl	[51]
GaN-HCG	1.7×10^{-3}	/	/	/	Ethanol	[52]
GaN-PhC	0.188	35	/	/	Water and oils	[53]
Porous-GaN Tamm plasmon	0.57	13	/	260	Water and air	[54]
GaN Microdisk	5.4×10^{-6}	666.9	0.06	10923	NaCl	This work

adsorption and desorption of Na^+ on the sensor surface, and the Langmuir isotherm model is applicable in this study. The detailed explanation of the polarization characteristics of GaN-based materials is provided by the Figure S8 (Supporting Information).

The detection limit (DL) is another important parameter which is used to accurately measure the minimum change in refractive index of solution samples. DL is defined as:

$$DL = \frac{R}{S} \tag{5}$$

where R represents the sensor resolution (the smallest detectable change in resonant wavelength), and S denotes the sensor sensitivity.[49] The sensor resolution R is positively correlated with the total system noise σ_{total} ($R = 3\sigma_{total}$). And the total system noise σ_{total} can be experimentally examined by measuring the standard deviation of the wavelength fluctuation from a reference blank sample. The standard deviation of the lasing wavelength fluctuation of the reference microdisk was measured to be ≈0.00119 nm, which can be reasonably regarded as σ_{total} for this study (Figure S9, Supporting Information). According to equation 5, a $DL_{(low)} = 5.4 \times 10^{-6}$ RIU can be obtained for Mode 8 in the low concentration range. Even in the high concentration range, Mode 8 maintains an excellent detection limit $DL_{(high)} = 3.1 \times 10^{-4}$ RIU. **Table 2** shows the comparison of S, DL and other values for RI sensors reported in previous studies and the values in this work. The S and DL in this study are among the best values in reported researches. These findings demonstrate that the flexible GaN-based microdisk lasers are highly sensitive to minute variations in the external environment. The high sensitivity and low detection limit highlight the valuable refractive index optical sensing capabilities of the flexible GaN-based microdisk lasers.

3. Conclusion

In summary, we present a novel secondary substrate transfer technique, serving as a crucial method to achieve high-performance flexible GaN-based microdisk lasers on PDMS substrate. The microdisk lasers exhibit a Q-factor of approximately 10 923 at room temperature, with a narrow linewidth of 0.045 nm and a threshold energy of approximately 312.31 μJ cm^{-2}. The lasing spectra of the microdisk lasers can be linearly modulated by varying the stress in the PDMS substrate and altering the refractive index of the surrounding environment, respectively, demonstrating their potential for dual-modal applications in micro optical sensing. The device as a strain optical sensor achieves a sensitivity of 0.08 nm/mm^{-1}, while as a refractive index optical sensor demonstrates a maximum sensitivity of 666.9 nm/RIU, with a detection limit ranging from $DL_{(low)} = 5.4 \times 10^{-6}$ RIU to $DL_{(high)} = 3.1 \times 10^{-4}$ RIU. We believe that flexible GaN-based microdisk lasers with excellent optical performance and dual-modal sensing characteristics have broad prospects for extensive applications in the field of multifunctional optical sensing.

4. Experimental Section

Sensor Fabrication: The manufacturing process of flexible GaN microdisk lasers can be provided by Figure 1. Figure S1 in the supporting information shows the structure of the epitaxial wafer and its cross-sectional SEM image. For detailed process steps, please refer to Device fabrication. During the first substrate transfer, photoresist was used as the bonding filler material between the GaN epitaxy and the Si substrate. Subsequently, a KrF excimer laser was used as the light source (wavelength 248 nm, repetition rate 1 Hz, pulse width 25 ns, laser energy density 1.413 J cm^{-2}) for the delamination of the sapphire substrate. After ICP etching the microdisk mesa, a BOE solution containing 49% HF was used to remove the SiO_2 layer. Under constant temperature conditions of 40 °C, the entire structure after forming the microdisk surfaces was immersed in the prepared BOE solution. The sample was rotated uniformly to ensure sufficient contact with the etching solution. After 8 minutes of etching, the SiO_2 layer was completely removed. Finally, the GaN microdisks on the Si substrate were immersed in acetone solution and maintain it in a water bath at 50 °C for 3 hours. After the water bath, the sample was removed and immediately flipped to bond onto the PDMS substrate. The PDMS substrate was peeled off, completing the fabrication of the flexible GaN-based microdisk lasers.

Structural Characterization: GaN epitaxial wafer cross-section and GaN microdisk morphology were characterized by a dual-beam focused scanning electron microscope system (FIB-SEM).

Optical Measurement: A 355 nm pulsed laser model CryLas FTSS-355 Q1 with a pulse width of 1 ns and a repetition frequency of 15 KHz was used as the pump source at room temperature. The relationship between tensile stress, different concentrations of NaCl solutions and the excitation spectral shift of GaN microdisks was characterized using the μ-PL measurement system. Raman spectra were recorded by laser confocal Raman microscopy with an excitation wavelength of 633 nm. strain sensing experiments were performed using a homemade test displacement stage, and refractive index sensing experiments were performed using interval measurements.

Supporting Information

Supporting Information is available from the Wiley Online Library or from the author.

Acknowledgements

H.Z. and L.M. contributed equally to this work. This work was supported by National Natural Science Foundation of China (No. 62474150, U21A20493, 62234011), and Natural Science Foundation of Fujian Province (NO. 2023J05020).

Conflict of Interest

The authors declare no conflict of interest.

Data Availability Statement

The data that support the findings of this study are available from the corresponding author upon reasonable request.

Keywords

dual-modal, flexible substrate, GaN microdisk, refractive index optical sensor, strain optical sensor

Received: January 16, 2025
Revised: March 20, 2025
Published online:

[1] Y. Liu, Y. Li, M. Y. Li, J. J. He, *Opt. Express* **2017**, *25*, 000972.
[2] J. B. Khurgin, M. A. Noginov, *Laser Photon. Rev.* **2021**, *15*, 2000250.
[3] P. Michler, A. Kiraz, L. D. Zhang, C. Becher, E. Hu, A. Imamoglu, *Appl. Phys. Lett.* **2000**, *77*, 126918.
[4] F. Tabataba-Vakili, L. Doyennette, C. Brimont, T. Guillet, S. Rennesson, E. Frayssinet, B. Damilano, J. Y. Duboz, F. Semond, I. Roland, M. El Kurdi, X. Checoury, S. Sauvage, B. Gayral, P. Boucaud, *ACS Photonics* **2018**, *5*, 8b00542.
[5] Y. J. Wang, H. Zhang, S. X. Duan, W. Lin, B. Liu, J. X. Wu, *IEEE Sens. J.* **2021**, *21*, 3045149.
[6] Y. Mei, M. Xie, H. Long, L. Ying, B. Zhang, *J. Lightwave Technol.* **2022**, *40*, 3147803.
[7] M. Humar, S. H. Yun, *Nat. Photonics* **2015**, *9*, 129.
[8] F. Vollmer, S. Arnold, *Nat. Methods* **2008**, *5*, 1221.
[9] Z. Y. H. Wang, Y. F. Zhang, X. R. Gong, Z. Y. Yuan, S. L. Feng, T. H. Xu, T. G. Liu, Y. C. Chen, *Nanoscale Adv.* **2020**, *2*, 00107d.
[10] A. Capocefalo, S. Gentilini, L. Barolo, P. Baiocco, C. Conti, N. Ghofraniha, *Photonics Res.* **2023**, *11*, 477139.
[11] I. Brice, K. Grundsteins, A. Atvars, J. Alnis, R. Viter, A. Ramanavicius, *Sens. Actuator B-Chem.* **2020**, *318*, 128004.
[12] J. L. Sun, W. Q. Mao, C. S. Xia, W. A. Wang, Q. N. Cui, Z. L. Shi, G. Y. Zhu, M. L. Wang, C. X. Xu, *Adv. Opt. Mater.* **2024**, *12*, 2301989.
[13] T. Kouno, M. Sakai, K. Kishino, K. Hara, *Opt. Lett.* **2015**, *40*, 2866.
[14] M. Schubert, L. Woolfson, I. R. M. Barnard, A. M. Dorward, B. Casement, A. Morton, G. B. Robertson, P. L. Appleton, G. B. Miles, C. S. Tucker, S. J. Pitt, M. C. Gather, *Nat. Photonics* **2020**, 452, *14*, s41566-020-0631-z.
[15] J. W. Wang, A. W. Poon, presented at IEEEConference on Lasers and Electro-Optics, (CLEO), San Jose, CA **2015** May.
[16] J. W. Wang, Z. S. Yao, A. W. Poon, *Front. Mater.* **2015**, *2*, 00034.
[17] I. Molina-Fernández, J. Leuermann, A. Ortega-Moñux, J. G. Wangüemert-Pérez, R. Halir, *Opt. Express* **2019**, *27*, 12616.
[18] H. Xu, J. Zhang, K. M. Davitt, Y. K. Song, A. V. Nurmikko, *J. Phys. D-Appl. Phys.* **2008**, *41*, 094013.
[19] C. L. Deng, Q. L. Zhao, Y. C. Gan, C. S. Yang, H. B. Zhu, S. M. Mo, J. J. Zheng, J. L. Li, K. Jiang, Z. M. Feng, X. M. Wei, Q. Y. Zhang, Z. M. Yang, S. H. Xu, *Biosens. Bioelectron.* **2023**, *241*, 115667.
[20] K. Chung, C. H. Lee, G. C. Yi, *Science* **2010**, *330*, 1195403.
[21] Y. Mei, M. C. Xie, H. Xu, H. Long, L. Y. Ying, B. P. Zhang, *Opt. Express* **2021**, *29*, 416873.
[22] Y. X. Yao, Y. Liang, J. B. Guo, H. X. Xiu, *Semicond. Sci. Technol.* **2023**, *38*, 074001.
[23] G. Y. Zhu, F. F. Qin, X. Li, Y. Sun, F. Gao, M. F. Tian, B. J. Ji, Y. J. Wang, *Front. Mater.* **2022**, *9*, 845885.
[24] J. Wang, M. X. Feng, R. Zhou, Q. Sun, J. X. Liu, Y. N. Huang, Y. Zhou, H. W. Gao, X. H. Zheng, M. Ikeda, H. Yang, *Photonics Res.* **2019**, *7*, 000b32.
[25] Y. J. Tang, M. X. Feng, H. R. Zhao, J. Wang, J. X. Liu, X. J. Sun, Q. Sun, S. M. Zhang, H. Yang, *Opt. Express* **2022**, *30*, 455620.
[26] T. Yang, Y. H. Chen, Y. C. Wang, W. Ou, L. Y. Ying, Y. Mei, A. Q. Tian, J. P. Liu, H. C. Guo, B. P. Zhang, *Nano-Micro Lett.* **2023**, *15*, 223.
[27] Y. Y. Peng, J. F. Lu, D. F. Peng, W. D. Ma, F. T. Li, Q. S. Chen, X. D. Wang, J. L. Sun, H. T. Liu, C. F. Pan, *Adv. Funct. Mater.* **2019**, *29*, 1905051.
[28] P. Hu, Y. F. Li, S. N. Zhang, Y. Zhang, Z. H. Tian, F. Yun, *CrystalsCrystals* **2021**, *11*, 1251.
[29] K. H. Li, Y. F. Cheung, H. W. Choi, *ACS Appl. Electron. Mater.* **2019**, *1*, 9b00114.
[30] P. Gu, S. Yang, L. L. Ma, T. Yang, X. Hou, Y. Mei, L. Y. Ying, *Opt. Lett.* **2023**, *48*, 496680.
[31] H. Yixiao, G. Hua, H. Jianxun, presented at 2021 5th International Conference on Mechanics, Mathematics and Applied Physics (ICMMAP 2021), Guilin, China **2021** (July).
[32] X. P. Ou, Y. Qiu, M. Luo, J. J. Li, X. B. He, J. F. Gao, F. J. Sun, P. Zhang, G. Yang, A. Y. Du, B. Li, Z. C. Liu, Z. H. Li, L. Xie, X. Xiao, J. Luo, W. W. Wang, J. Tao, Y. Yang, *Adv. Mater. Technol.* **2024**, *9*, 2300998.
[33] A. Ahmed, Y. S. Guan, I. Hassan, C. Ling, Z. Li, I. Mosa, G. Phadke, P. R. Selvaganapathy, S. Q. Chang, S. Q. Ren, *Nano Energy* **2020**, *75*, 105044.
[34] Q. L. Hua, J. L. Sun, H. T. Liu, R. R. Bao, R. M. Yu, J. Y. Zhai, C. F. Pan, Z. L. Wang, *Nat. Commun.* **2018**, *9*, 244.
[35] T. Q. Trung, S. Ramasundaram, B. U. Hwang, N. E. Lee, *Adv. Mater.* **2016**, *28*, 1504441.
[36] P. Steglich, D. G. Rabus, C. Sada, M. Paul, M. G. Weller, C. Mai, A. Mai, *IEEE Sens. J.* **2022**, *22*, 10089.
[37] T. Liu, D. Li, H. Hu, X. Huang, Z. F. Zhao, W. Sha, C. Y. Jiang, C. H. Du, M. M. Liu, X. Pu, B. Ma, W. G. Hu, Z. L. Wang, *Nano Energy* **2020**, *67*, 104218.
[38] Y. M. Banad, S. M. A. Hasan, S. S. Sharif, G. Veronis, M. R. Gartia, *Nano Sel.* **2024**, *5*, 2300184.
[39] J. Sellés, V. Crepel, I. Roland, M. El Kurdi, X. Checoury, P. Boucaud, M. Mexis, M. Leroux, B. Damilano, S. Rennesson, F. Semond, B. Gayral, C. Brimont, T. Guillet, *Appl. Phys. Lett.* **2016**, *109*, 231101.
[40] C. Y. Zhao, C. W. Tang, J. N. Wang, K. M. Lau, *Appl. Phys. Lett.* **2020**, *117*, 031104.
[41] I. Goykhman, B. Desiatov, U. Levy, *Appl. Phys. Lett.* **2010**, *97*, 081108.
[42] J. T. Gohring, P. S. Dale, X. D. Fan, *Sens. Actuator B-Chem.* **2010**, *146*, 226.
[43] M. D. LeVan, T. Vermeulen, *J. Phys. Chem.* **1981**, *85*, 3247.
[44] M. R. Foreman, J. D. Swaim, F. Vollmer, *Adv. Opt. Photonics* **2015**, *7*, 168.
[45] H. Jeong, S. Y. Jeong, D. J. Park, H. J. Jeong, S. Jeong, J. T. Han, H. J. Jeong, S. Yang, H. Y. Kim, K. J. Baeg, S. J. Park, Y. H. Ahn, E. K. Suh, G. W. Lee, Y. H. Lee, M. S. Jeong, *Sci. Rep.* **2015**, *5*, 7778.

[46] C. G. Zhang, W. L. Wang, X. D. Hao, Y. Peng, Y. L. Zheng, J. Liu, Y. Y. Kang, F. J. Zhao, Z. T. Luo, J. J. Guo, B. S. Xu, L. Q. Shao, G. Q. Li, *Adv. Funct. Mater.* **2021**, *31*, 2007487.
[47] M. Tautz, M. T. Kuchenbrod, J. Hertkorn, R. Weinberger, M. Welzel, A. Pfitzner, D. D. Díaz, *Beilstein J. Nanotechnol.* **2020**, *11*, 41.
[48] Y. P. Sui, B. Wang, Z. D. Zhao, W. Xu, X. L. Li, X. Z. Wang, G. H. Yu, *J. Cryst. Growth* **2014**, *394*, 11.
[49] I. M. White, X. D. Fan, *Opt. Express* **2008**, *16*, 1020.
[50] D. Kim, P. Popescu, M. Harfouche, J. Sendowski, M. E. Dimotsantou, R. C. Flagan, A. Yariv, *Opt. Lett.* **2015**, *40*, 4106.
[51] X. K. Wang, X. W. Guan, Q. S. Huang, J. J. Zheng, Y. C. Shi, D. X. Dai, *Opt. Lett.* **2013**, *38*, 5405.
[52] Y. Takashima, M. Haraguchi, Y. Naoi, *Sensors* **2020**, *20*, 4444.
[53] L. Zhang, T. Cao, Z. G. Lia, K. R. Qin, W. P. Yan, presented at Conference on Advanced Sensor Systems and Applications V, Beijing, P. R China, **2012** (Nov.).
[54] P. S. Maji, G. Banerjee, S. Acharyya, A. R. Maity, *Opt. Quantum Electron.* **2022**, *54*, 623.